Ab initio study of electronic and magnetic properties of the C-codoped $Ga_{1-x}Mn_xN$ $(10\bar{1}0)$ surface

Q. Wang, Q. Sun, and P. Jena
Physics Department, Virginia Commonwealth University, Richmond, Virginia 23284, USA
(Received 8 September 2006; published 16 January 2007)

First principles calculations based on gradient corrected density functional theory have been carried out to study the magnetic coupling between Mn atoms in pure and carbon doped $Ga_{1-x}Mn_xN$ thin films. We show that the ground state of Mn-doped GaN $(10\bar{1}0)$ thin film, with Mn replacing the Ga sites, is antiferromagnetic but becomes ferromagnetic when it is codoped with C. The interaction between the Mn spins via the delocalized holes introduced by codoping of C at N sites is responsible for this transition. The overlap between Mn $3d$ and C $2p$ in the spin-up band renders half-metallic character to the C codoped (Ga,Mn)N system. The observed ferromagnetism in (Ga,Mn)N thin films is believed to be associated with defects or codoping with other elements during the film growth. The present study provides the theoretical understanding for many recent experiments on the Mn-doped GaN system.

DOI: 10.1103/PhysRevB.75.035322 PACS number(s): 71.55.−i, 75.50.Pp, 71.15.Mb, 36.40.Cg

I. INTRODUCTION

The study of ferromagnetism in (Ga, Mn)As[1] and the theoretical prediction that Mn-doped GaN could be ferromagnetic (FM) at or above room temperature,[2] have led to intensive research on transition metal elements doped (III, V) dilute magnetic semiconductors (DMSs).[3–19] This interest is fueled by the possibility that both charge and spin of electrons can be manipulated for potential applications in spintronics devices as well as in a new generation of low-power-consumption electronics, nonvolatile memories, and field-configurable logic devices. Among the various DMS materials, Mn-doped GaN is particularly interesting because GaN is a direct wide energy band gap semiconductor with high thermal, chemical, and mechanical stability. In addition, Mn-doped GaN is one of the few materials where magnetism above room temperature has been reported and is extensively studied. However, there is considerable controversy in the reported results. The nature and origin of the magnetic coupling in this material continue to be hotly debated issues. The mechanism for the observed magnetic behavior is complex and appears to depend on a number of factors, including the sample preparation conditions, defects, Mn-Mn separation, and carrier density and type. It has been shown that the coupling between two Mn atoms in bulk GaN is FM while that on the $(11\bar{2}0)$ surface is antiferromagnetic (AFM) due to bond length contraction on the surface.[11] An interesting question then arises: Is it possible that the coupling between Mn atoms substituted on different surfaces of GaN may exhibit FM ordering since the Mn-Mn distances are likely to be different for different surface orientations? If this is the case, Mn-doped GaN nanoparticles may have some potential as a DMS material since different surface orientations may be manifested in the same particle.

In this paper, we present a detailed study of the electronic and magnetic properties of Mn-doped GaN thin films having $(10\bar{1}0)$ orientation and the wurtzite structure to demonstrate the effect of surface orientation on the magnetic coupling between Mn atoms. In addition, we have also studied the effect of carbon codoping on the magnetic properties of $Ga_{1-x}Mn_xN$ $(10\bar{1}0)$ thin films as a function of Mn concentration. The calculations of total energies, electronic structure, and magnetic coupling for different Mn doping concentrations with and without C codoping are carried out using spin polarized density functional theory (DFT)[20] and generalized gradient approximation (GGA)[21] for exchange and correlation. We show that pure $Ga_{1-x}Mn_xN$ thin films with Mn atoms substituting Ga sites are AFM, and this coupling is insensitive to the Mn concentration (from 4.2% to 12.5%). However, we find that C codoping can change the ground state from AFM to FM. The holes introduced by codoping C at N sites mediate the magnetic coupling between Mn atoms and the FM ordering can be tuned by controlling the hole concentration.

II. COMPUTATIONAL PROCEDURE

The GaN surface was modeled by a (2×2) ten-layer slab that contained 40 Ga atoms and 40 N atoms in the supercell (see Fig. 1). Each slab was separated from the other by a vacuum region of 10 Å in $[10\bar{1}0]$ direction. Tests were carried out by increasing the vacuum region up to 15 Å to ensure that the total energies have converged. The central four layers of the slab were held at their ideal bulk position while the three layers on either side of the slab were allowed to relax without any symmetry constraint. To preserve symmetry, the top and bottom layers of the slab have been taken to be identical in all the following calculations. The calculations of total energies and forces, and optimizations of geometry have been carried out using DFT and PW91 functional[22] for the GGA for exchange and correlation potential. A plane-wave basis set and the projector augmented wave (PAW) potentials[23] with the valence states $3d^{10}$, $4s^2$, and $4p^1$ for Ga; $3p^6$, $3d^5$, and $4s^2$ for Mn; $2s^2$ and $2p^3$ for N; and $2s^2$ and $2p^2$ for C, as implemented in the Vienna *Ab initio* Simulation Package (VASP),[24] were employed. The energy cutoff was set at 350 eV. The convergence in energy and force were set at 10^{-4} eV and 10^{-3} eV/Å, respectively.

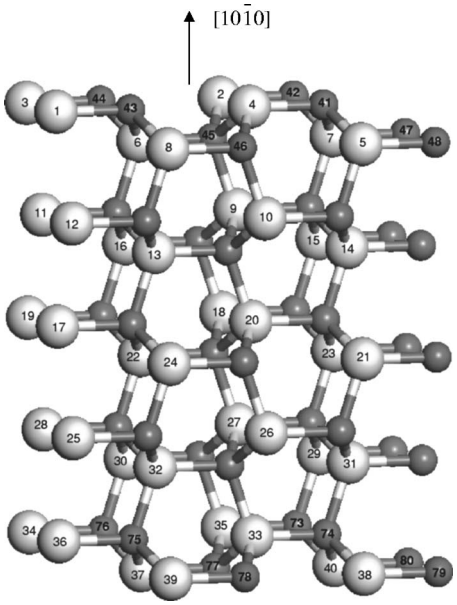

FIG. 1. The schematic representation of a ten-layer slab model for wurtzite GaN (10$\bar{1}$0) surface, which consists of 40 Ga and 40 N atoms. The larger and lighter spheres are Ga, the smaller and darker spheres are N.

The k-point convergence was achieved with $(7\times5\times1)$ Monkhorst-Pack grid[25] although tests with up to $(8\times6\times2)$ Monkhorst k-points mesh were carried out to ensure accuracy.

III. RESULTS AND DISCUSSIONS

The electronic and magnetic properties of Mn-doped and C and Mn codoped GaN thin films have been studied in successive steps. First, the electronic structure and surface reconstruction of the pure GaN (10$\bar{1}$0) thin film was calculated. Second, we studied Mn-doped GaN (10$\bar{1}$0) by determining the preferred sites of the Mn atoms and the magnetic coupling between them as a function of Mn concentration. Finally, the effect of C codoping on the magnetic properties of $Ga_{1-x}Mn_xN$ was calculated.

A. Electronic structure and surface reconstruction of pure GaN (10$\bar{1}$0) surface

The (10$\bar{1}$0) surface is nonpolar and could be prepared by cleaving or an epitaxial growth process. The surface reconstruction was carried out by fully optimizing the geometry of the ten-layer GaN slab. Our results for the equilibrium lattice constants $a=3.185$ Å and $c=5.182$ Å are in very good agreement with experimental results.[26] The relaxation energy defined as the difference in the total energies of the relaxed and ideal surface configurations was found to be 3.511 eV. This corresponds to an energy gain of 0.146 eV/Ga-N dimer, which is comparable with that in the (11$\bar{2}$0) GaN surface.[11] The Ga atoms on the surface layer move inward by −0.125 Å while those on the second and third layers move outward by 0.178 Å and 0.014 Å, respectively. Meanwhile, the N atoms move outward, respectively, by 0.157 Å, 0.089 Å, and 0.05 Å for the atoms on the surface, second, and third subsurface layers. This is in agreement with the general description of nonpolar semiconductor surfaces in which anions move outward and cations move inward with respect to the unrelaxed surface plane. The vertical buckling $\perp_{1\Delta}$ of Ga-N dimer on the surface atomic layer is 0.282 Å. The bond length of Ga-N on the surface layer along the [0001] direction is 1.846 Å (leading to a contraction of −6.91%), while those on the subsurface and the third layer are 1.961 Å and 1.967 Å (leading to a contraction of −1.20% and −1.13%, respectively). These results are in good agreement with previous first principles pseudopotential calculations on the GaN (10$\bar{1}$0) surface.[27]

The total electronic density of states (DOS) for spin-up and spin-down electrons corresponding to the undoped GaN (10$\bar{1}$0) supercell is plotted in Fig. 2(a_1). The partial DOS of Ga and N atoms are plotted in Figs. 2(a_2) and 2(a_3), respectively. From the total spin DOS, we note that the valance band comes essentially from N $2p$ with small contributions from the Ga $3p$ and $4s$ orbitals and a negligible contribution from the Ga $3d$ and N $2s$ orbital. The conduction band is composed of Ga $3p$, $4s$, and N $2p$ with small contributions from Ga $3d$ and N $2s$. Fermi level is located in the gap region, indicating that the GaN (10$\bar{1}$0) thin film is a semiconductor. In addition, the DOS curves for spin-up and spin-down are totally symmetric, therefore there is no net magnetic moment in this system.

The calculations on the six-, eight-, and twelve-layer slabs of (2×2) (10$\bar{1}$0) GaN surface, corresponding respectively to 48, 64, and 96 atoms/supercell, have also been carried out to check the convergence of the electronic structure. The distances between the topmost and bottommost layers for the six-, eight-, and twelve-layer slabs are 6.444, 9.206, and 14.729 Å, respectively. The outermost two layers on either side of the six-layer slab and three layers of the eight- and twelve-layer slabs were allowed to relax without any symmetry constraint. The relaxation energies were found to be, respectively, 2.272, 3.508, and 3.513 eV for the six-, eight-, and twelve-layer slab corresponding to an energy gain of 0.142 eV/Ga-N dimer for the six-layer slab and 0.146 eV/Ga-N dimer for the other two slabs. It is important to note that the relaxed Ga-N bond lengths along the [0001] direction for all the slabs with the different thickness (from six layers to twelve layers) have the same value, namely 1.846 Å and 1.961 Å in the surface and subsurface layer, respectively. This indicates that a six-layer slab is adequate to study the effects of surface.

B. Mn-doped GaN (10$\bar{1}$0) surface

We now present our results on the Mn-doped GaN slabs. First we determined the preferred site of Mn atoms in the GaN (10$\bar{1}$0) thin film. This was achieved by substituting a single Ga atom with one Mn at different sites, i.e., at a surface site No. 4, at a subsurface site No. 6, and then at a third layer site No. 9 in Fig. 1, respectively. To preserve the sym-

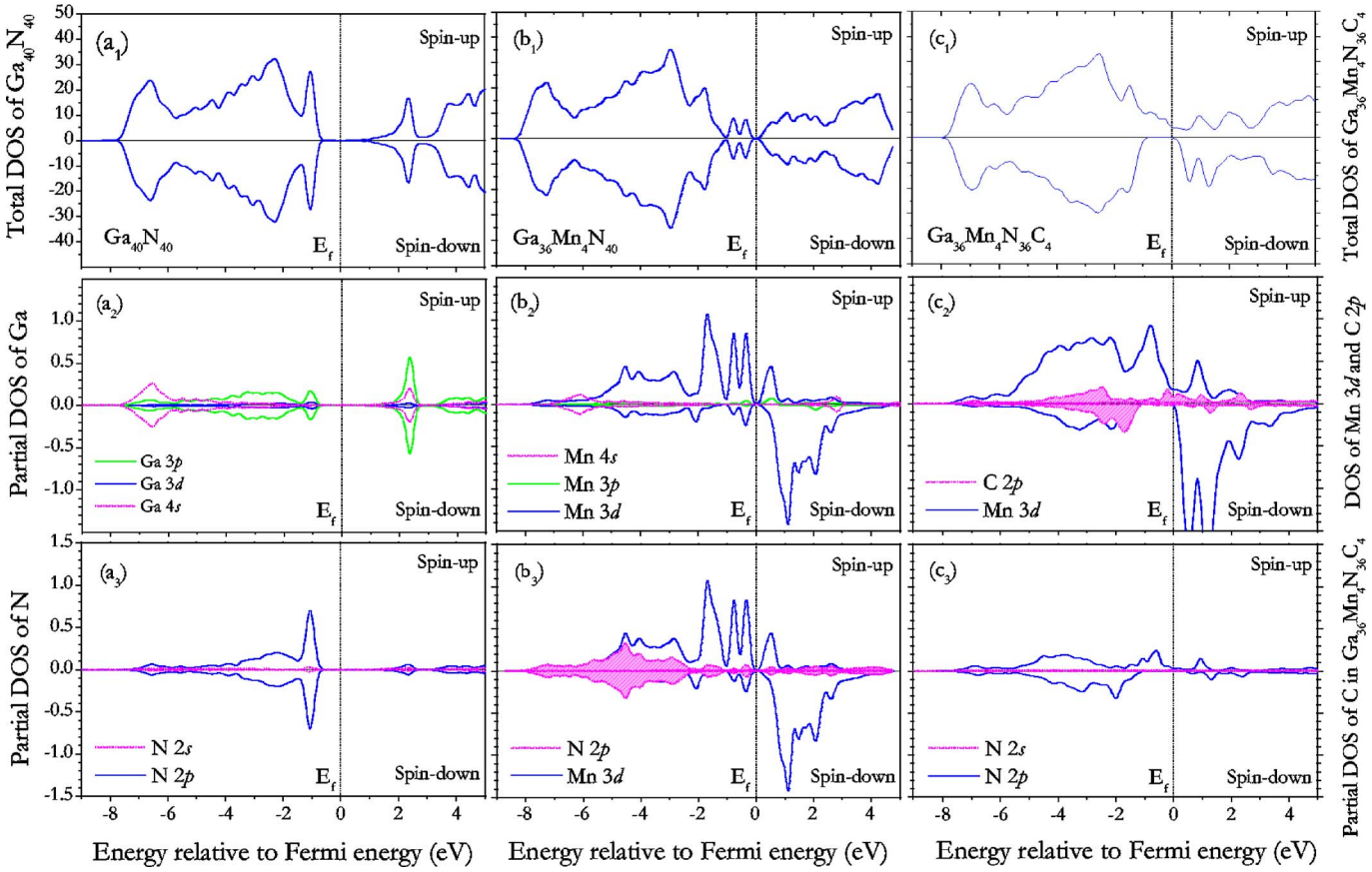

FIG. 2. (Color online) (a_1) Total DOS, (a_2) partial DOS of Ga, and (a_3) partial DOS of N corresponding to undoped wurtzite ($10\bar{1}0$) GaN surface slab supercell $Ga_{40}N_{40}$. (b_1) Total DOS, (b_2) partial DOS of Mn, and (b_3) partial DOS of Mn 3*d* and neighboring N 2*p* for $Ga_{36}Mn_4N_{40}$ supercell. (c_1) Total DOS, (c_2) partial DOS of Mn 3*d* and neighboring C 2*p*, and (c_3) partial DOS of N for C-codoped $Ga_{36}Mn_4N_{36}C_4$ supercell.

metry, the corresponding sites No. 37, No. 33, or No. 32 on the bottom three layers of the slab were replaced with Mn, correspondingly. This led to a supercell consisting of $Ga_{38}Mn_2N_{40}$ and a Mn concentration of 5.00%. The total energy calculation and the geometry optimization for these three configurations show that the Mn atom has a clear preference for the surface site over the interior sites irrespective of whether the film is allowed to relax or not. In the absence of any geometrical relaxation, Mn atom residing on the surface layer lies 0.486 eV and 1.123 eV lower in energy than that when it occupies the second and the third layers, respectively. These energies change respectively to 1.099 eV and 1.468 eV when the structure is relaxed. In the Mn-doped GaN ($11\bar{2}0$) film surface,[11] it was also found that the surface substituted site lies 1.37 eV and 1.54 eV below that of the subsurface and third layer sites, respectively. The relaxed Mn-N bond length along the [0001] direction, in the ground state, is found to be 1.797 Å, which contracted by −2.65%, as compared to that in relaxed pure GaN surface. The magnetic moment on the Mn atom at surface site is $3.374\mu_B$ and mainly arises from Mn 3*d* ($3.285\mu_B$) orbital with small contributions from Mn 4*s* ($0.05\mu_B$) and Mn 4*p* orbitals ($0.04\mu_B$). The moment of Mn atom in the subsurface and the third layer is $3.405\mu_B$ and $3.416\mu_B$, respectively. The charge density distribution in the plane containing the Mn and the neighboring N atom is plotted in Fig. 3(a) and shows that there is an observable interaction between the Mn and the neighboring N atom.

Next, we studied the magnetic coupling between the Mn atoms in the GaN ($10\bar{1}0$) thin film. To this end, we substituted two Ga atoms with two Mn on both top and bottom sides of the $Ga_{40}N_{40}$ slab. Consequently, a total replacement of four Ga atoms with four Mn atoms results in a 10.00% Mn doping concentration and a $Ga_{36}Mn_4N_{40}$ supercell. There are many ways Mn atoms can replace Ga atoms at different sites on the surface and/or subsurface or third layer sites. We have considered six different configurations here, because it was demonstrated above that a single Mn atom prefers to occupy the surface site. We have specified the six configurations in the first column of Table I by giving the sites where the Ga atoms are replaced by Mn (see Fig. 1). For example, configuration I represents the replacement of the nearest neighbor Ga atoms with Mn at sites (No. 2, No. 4) on the surface layer, and of the corresponding symmetrical Ga sites (No. 39, No. 37) on the bottom layer in Fig. 1. Geometry optimization and total energy calculations were carried out for all these six configurations. For each configuration we studied the FM and AFM coupling between the Mn atoms to determine the most preferred geometrical and magnetic state. The magnetic moments located on each Mn atom and the *spd*- and the site projected wave function character have been

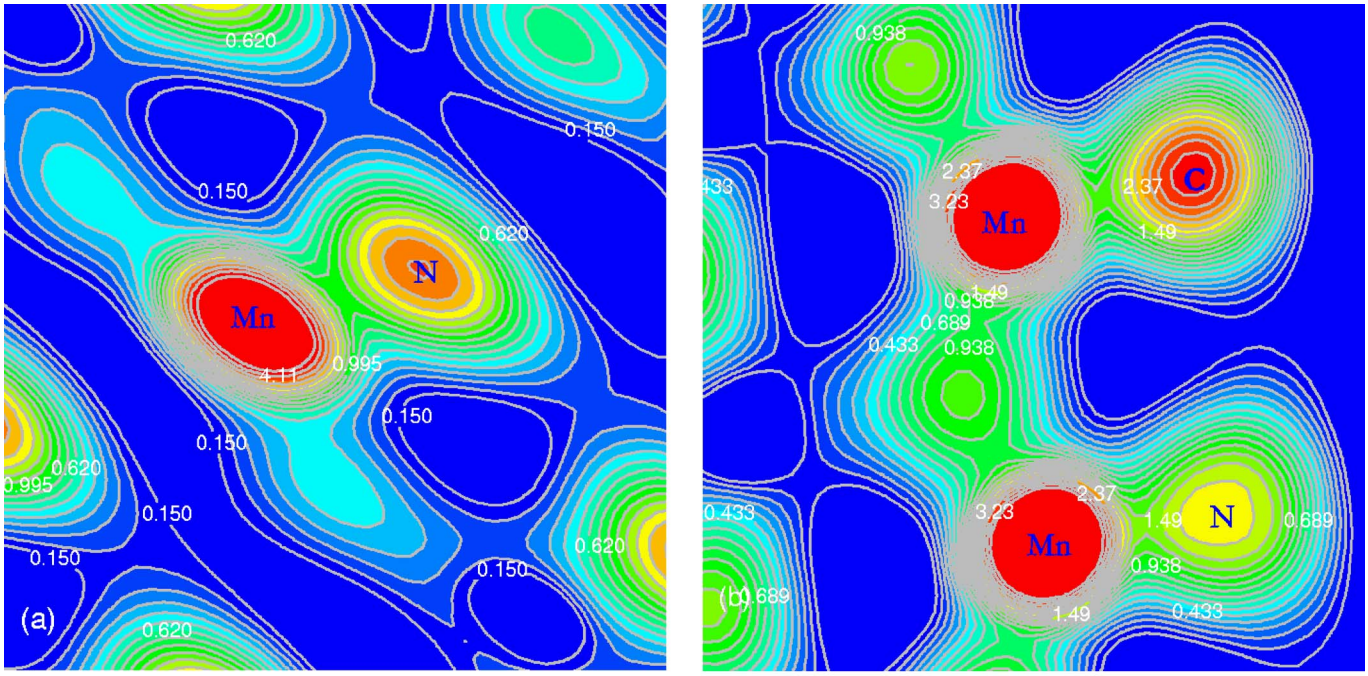

(a) (b)

FIG. 3. (Color online) Charge density distribution of (a) $Ga_{38}Mn_2N_{40}$, and (b) $Ga_{36}Mn_4N_{36}C_4$ supercells in the plane containing Mn, C, and neighboring N atoms.

calculated self-consistently for all the configurations. The main results are summarized in Table I. It is found that configuration I is the ground state with the AFM coupling lying 0.541 eV lower in energy than the FM one, where the two Mn atoms reside in the surface layer sites, and cluster around N atoms. The optimized Mn-N bond length along the [0001] direction is 1.798 Å, corresponding to a contraction of −2.6% as compared to that for the undoped GaN surface. The Mn-Mn distance of 3.189 Å, however, is unchanged from the corresponding Ga-Ga distance in the undoped case. The relative energies $\Delta\varepsilon$ calculated with respect to the ground state are listed in the second column. The energy difference ΔE between the AFM and FM states [$\Delta E = E(\text{AFM})\text{-}E(\text{FM})$] are given in the third column, which determines the preferred magnetic coupling between the two Mn atoms. The negative ΔE means that the AFM state is lower in energy. The preferred magnetic coupling, the optimized bond length between Mn and its nearest neighbor N along the [0001] direction, and the optimized Mn-Mn distance are collected in the last three columns of Table I.

Comparing the relative energies, we note that the total energy increases as the Mn atoms move from surface layer to the interior sites of the film. Configuration V and VI, where the two Mn atoms occupy respectively the subsurface and the third layer sites, are found to be 2.307 eV and 3.228 eV higher in energy than the ground state, respectively. This shows again that Mn atoms prefer the surface sites and this site preference is not affected by the Mn concentration. The relative energies corresponding to configuration II and III, where the Mn atoms reside in the next nearest sites (No. 1, No. 4) and the further sites (No. 1, No. 2), show that these two configurations also lie higher in energy than the ground

TABLE I. The first column identifies the Ga sites in Fig. 1 that are placed by Mn. $\Delta\varepsilon$ is the relative energy calculated with respect to the ground state (configuration I) of $Ga_{36}Mn_4N_{40}$. ΔE is the energy difference between the AFM and FM states ($\Delta E = E_{\text{AFM}} - E_{\text{FM}}$). $d_{\text{Mn-N}}$ is the optimized bond length between Mn and its nearest neighboring N along the [0001] direction, and $d_{\text{Mn-Mn}}$ is the optimized distance between the two Mn atoms.

Configurations	$\Delta\varepsilon$ (eV)	ΔE (eV)	Coupling	$d_{\text{Mn-N}}$ (Å)	$d_{\text{Mn-Mn}}$ (Å)
I (2,4/38,40)	0	−0.541	AFM	1.798(−9.65%)	3.189
II (1,4/37,40)	1.084	0.096	FM	1.813(−8.89%)	5.185
III (1,2/37,38)	1.178	0.002	FM	1.816(−8.74%)	6.087
IV (4,8/40,35)	1.795	−0.047	AFM	1.835(−7.79%)	2.969
V (6,8/33,35)	2.307	0.113	FM	1.973(−0.85%)	3.189
VI (9,10/32,30)	3.228	0.084	FM	1.975(−0.75%)	3.189

state configuration. This indicates that Mn atoms prefer to cluster in the GaN surface. Meanwhile, it is interesting to note that although the Mn-Mn distances in configuration I, V, and VI have the same value ($d_{\text{Mn-Mn}}$=3.189 Å), their corresponding Mn-N bond lengths are quite different, namely 1.798, 1.973, and 1.975 Å, respectively, and the magnetic couplings between the Mn atoms in these configurations are also different, i.e., the Mn atoms couple ferromagnetically in configuration V and VI with the FM state lying 0.113 eV and 0.084 eV lower in energy than their AFM states, respectively. The coupling in configuration I, on the other hand, is AFM. This demonstrates that at certain Mn-Mn distance, the contraction of Mn-N bond length plays a critical role in driving the AFM coupling between the Mn atoms. This is in agreement with the results obtained in our previous calculations on the $(11\bar{2}0)$ slab.[11] It is understandable that the energy difference, ΔE between the AFM and FM states decreases as the Mn-Mn distance increases. For instance, in configuration I, the two Mn atoms form the nearest neighbor on the surface layer, they are 3.189 Å apart, and ΔE =−0.135 eV/Mn atom. However, when the distance between them is 5.185 and 6.078 Å in configuration II and III, the ΔE is 0.019 and 0.001 eV/Mn atom, respectively. Thus, one can conclude that in the dilute limit when the distance between Mn atoms is far apart, the Mn-doped GaN thin film system can display FM, paramagnetic or spin glass behavior, as there is no preferential direction for the spin to align. This explains the variety of magnetic behavior observed in different experiments.[3–6,14–17]

The total DOS for the ground state configuration I, and the corresponding partial DOS of Mn atom and the partial DOS for Mn 3*d* and N 2*p* are plotted in Fig. 2(b_1), Fig. 2(b_2), and Fig. 2(b_3), respectively. We note that the total DOS for spin-up and spin-down are again identical leading to zero magnetic moment, although the energy gap is sufficiently reduced from that in the undoped GaN, see Fig. 2(a_1). The magnetic moment on each Mn atom is $3.05\mu_B$ and mainly comes from the Mn 3*d* orbital ($2.95\mu_B$). Small contributions to the moment also arises from the Mn 3*p* ($0.03\mu_B$) and Mn 4*s* ($0.1\mu_B$) orbitals due to the *sp* and *d* hybridization, as shown in Fig. 2(b_2). The neighboring N atom of Mn is polarized antiferromagnetically with a magnetic moment of $0.06\mu_B$ which mainly comes from N 2*p* orbitals ($0.05\mu_B$), see Fig. 2(b_3). The average magnitude of magnetic moment (as there is a slight difference when the two Mn atoms reside in different layers) on the Mn atom for each configuration is given in Fig. 4, which close to $3\mu_B$.

To study the effect of the Mn concentration on the magnetic coupling between the Mn atoms, we performed the extensive calculations on the GaN slabs with different thickness along the $[10\bar{1}0]$ direction, as well as the $[01\bar{1}0]$ direction. At first, we increased the thickness of the slab to twelve layers based on the above (2×2) 10-layer slab along $[10\bar{1}0]$ direction to reach a lower Mn doping concentration. Thus, a slab supercell of $Ga_{48}N_{48}$ has been generated. To check the magnetic coupling between Mn atoms, we have also replaced two of the Ga atoms with Mn on either side of the slab at different sites on different layers, corresponding to

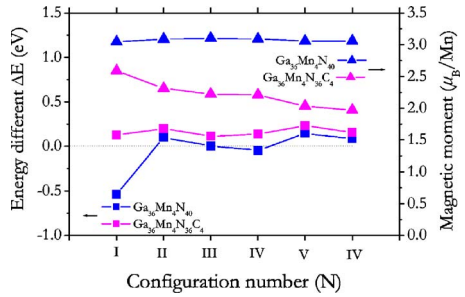

FIG. 4. (Color online) The energy difference ΔE between AFM and FM states and the average magnetic moment on Mn atom for the six configurations with and without C codoping. The six configurations are defined in Table I.

a 8.30% Mn doping concentration. The calculations have been carried out the same way as described above for the ten-layer slab. It was found that the configuration where the Mn atoms occupy the nearest neighboring Ga sites on the surface layer is again the ground state with the AFM state being 0.535 eV lower in energy than the FM state. We also find that Mn atoms prefer to reside on the GaN surface and cluster around N atoms. The magnetic moment on each Mn atom is found to be $3.05\mu_B$, and the moments located on the 3*p*, 3*d*, and 4*s* of Mn are nearly the same as those in the 10-layer slab. We also performed the calculations for the Mn-doped (2×2) 8-layer slab ($Ga_{32}N_{32}$) to reach a larger Mn concentration. The replacement of two Ga atoms with Mn on either side of the $Ga_{32}N_{32}$ slab generates a 12.5% Mn doping concentration. The ground state is once again found to be the configuration where the two Mn atoms reside on the nearest Ga surface sites, with the AFM state being lower in energy than the FM state. The energy difference ΔE and the local magnetic moment distributed on the Mn for this ground state are tabulated in Table II.

We then performed the calculations on changing the Mn concentration by increasing the slab thickness along the $[01\bar{1}0]$ direction. We note, in all the above (2×2) $(10\bar{1}0)$ surface slab models, the Mn atoms on the surface form a continuous chain along the $[01\bar{1}0]$ direction. One may wonder if the AFM coupling results from the formation of the Mn-Mn chains and if there is an interaction between the Mn atom and its image in the nearest supercell. To prevent the formation of the Mn-Mn chain, we used a (5×2) 6-layer slab containing 60 Ga atoms and 60 N atoms, in which the minimum distance between the Mn atom and its image in the nearest supercell is 10.07 Å along the $[01\bar{1}0]$ direction. In the calculations, the central two layers of this slab were fixed at the bulk crystalline position, while the top and bottom two layers were relaxed without any symmetry constraint. The geometry of the supercell was optimized fully by using (5×5×1) Monkhorst-Pack *k*-point mesh. When two Mn atoms are substitutionally doped at Ga sites on either side of the slab, a $Ga_{56}Mn_4N_{60}$ supercell with a 6.70% Mn concentration is formed. There are many more possible Ga sites for Mn atoms to replace, as there are more than twice the number of Ga-N dimers in each layer of this slab. We have carried out extensive search for the most favorable geometric

TABLE II. Composition of Mn-doped GaN slab, Mn concentration, the energy difference ΔE (ΔE_0) between the AFM and FM states, $\Delta E = E_{AFM} - E_{FM}$, with (without) geometry optimization, the magnetic moment on each Mn atom (in μ_B), the optimized nearest Mn-N bond length $d_{Mn\text{-}N}$ (in Å) along the [0001] direction, and the optimized Mn-Mn distance $d_{Mn\text{-}Mn}$ (in Å) for the supercells listed in the first column.

System	Slab layers	Mn concentration	ΔE_0 (eV)	ΔE (eV)	μ_{Mn}	$d_{Mn\text{-}N}$	$d_{Mn\text{-}Mn}$
$Ga_{28}Mn_4N_{32}$	(2×2)-8L	12.50%	−0.276	−0.549	3.01	1.799	3.189
$Ga_{36}Mn_4N_{40}$	(2×2)-10L	10.00%	−0.281	−0.541	3.05	1.798	3.189
$Ga_{44}Mn_4N_{48}$	(2×2)-12L	8.30%	−0.282	−0.535	3.05	1.798	3.189
$Ga_{56}Mn_4N_{60}$	(5×2)-6L	6.70%	0.040	−0.401	3.10	1.794	3.102
$Ga_{60}Mn_4N_{64}$	(4×2)-8L	6.25%	−0.001	−0.422	3.09	1.795	3.095
$Ga_{76}Mn_4N_{80}$	(4×2)-10L	5.00%	−0.010	−0.432	3.09	1.795	3.098
$Ga_{92}Mn_4N_{96}$	(4×2)-12L	4.20%	−0.034	−0.399	3.10	1.794	3.098

and magnetic configuration. Once again, we found that the Mn atoms prefer to reside in the nearest surface Ga sites and couple antiferromagnetically. The main results corresponding to the ground state are summarized in Table II. To further examine the magnetic coupling between Mn atoms in the dilute condition, we have also generated the 8-layer, 10-layer, and 12-layer (4×2) GaN $(10\bar{1}0)$ slabs, which correspond to $Ga_{64}N_{64}$, $Ga_{80}N_{80}$ and $Ga_{96}N_{96}$ supercells, respectively. The Mn doping concentrations of 6.25%, 5.00%, and 4.20% have been achieved by substituting two Ga atoms with Mn on either side of these slabs, respectively. In this way, no Mn-Mn chain can be formed along the $[01\bar{1}0]$ direction, and no interaction between the Mn atom and its image can occur. Using a (5×6×1) Monkhorst-Pack grid and the same procedure as described above, we found the results to be almost the same as those given in the smaller slabs; namely, the ground state is AFM and it lies about 0.1 eV/Mn atom lower in energy than the FM state, where the Mn atoms occupy the nearest surface sites of the Ga atoms and form clusters. The Mn-N bond length is about 1.8 Å. The magnetic moment on each Mn atom is about $3\mu_B$. The main results for the ground state configurations corresponding to each of the different thickness slabs are summarized in Table II. Computational details and results for other configurations are available upon request. The magnetic moment on the Mn atom and the bond length of Mn-N and Mn-Mn are comparable with those in the (2×2) slabs. In the fourth column of Table II, we also list the energy difference ΔE_0 between the AFM and FM states for the ground states configurations calculated without geometry optimization. Thus, it is clear that in the Mn-doped GaN $(10\bar{1}0)$ thin films, the AFM ordering at 0 K is energetically favorable, relative to the FM state, due to the Mn-N bond length contraction, and the magnetic coupling between Mn atoms is insensitive to the concentration of Mn over a wide range of concentration from 4.2% to 12.5%.

C. Mn and C codoped in GaN $(10\bar{1}0)$ surface

Finally, we have explored the possibility that the $Ga_{1-x}Mn_xN$ system when codoped with C could turn into a ferromagnet since replacing N with C would introduce hole carriers, which in turn could mediate the FM coupling between the Mn atoms. To this end, we have chosen a ten-layer (2×2) GaN slab codoped with Mn at Ga sites and C at N sites. We calculated the magnetic coupling between Mn atoms following the same procedure as performed for the $Ga_{1-x}Mn_xN$ systems. We replaced, respectively, one, two, and three N with C atoms on either side of the slab, generating corresponding supercells of $Ga_{36}Mn_4N_{38}C_2$, $Ga_{36}Mn_4N_{36}C_4$, and $Ga_{36}Mn_4N_{34}C_6$. For each of these C doping concentrations, we studied the energetics of the various configurations resulting from the replacement of the Ga and N at different sites with Mn and C, respectively. For

TABLE III. The supercells depicting the C-codoped (Ga,Mn)N 10-layer (2×2) slab, the N sites that were replaced by C (see Fig. 1), the energy difference ΔE (in eV) between AFM and FM states, the spin alignments of the two Mn atoms and the interlocking N or C atom (x) ("↑" means spin up and "↓" means spin down), the magnetic moment on each Mn atom and the x atom (in μ_B), and the optimized Mn-Mn distance (in Å) for each configuration.

System	Sites occupied by C	ΔE (eV)	Mn-x-Mn	μ_{Mn1}	μ_{Mn2}	μ_x	$d_{Mn\text{-}Mn}$
$Ga_{36}Mn_4N_{40}$	—	−0.541	↑-↑-↓	3.05	−3.05	0.01	3.189
$Ga_{36}Mn_4N_{38}C_2$	(45)	−0.180	↑-↑-↓	3.08	−2.27	−0.08	3.189
$Ga_{36}Mn_4N_{36}C_4$	(41,45)	0.124	↑-↓-↑	2.34	3.04	−0.17	3.191
$Ga_{36}Mn_4N_{34}C_6$	(41,42,45)	0.237	↑-↓-↑	2.39	2.39	−0.25	3.193

instance, we first replaced two Ga atoms with Mn at sites (No. 2, No. 4) and N with C at site No. 41 as shown in Fig. 1. The corresponding sites on the bottom layers were similarly replaced to preserve the symmetry. The geometry optimization and total energy calculations for the FM and AFM spin alignments have been carried out. The N atom at sites No. 45 and No. 46 were replaced by C respectively, but still keeping the two Mn at sites (No. 2, No. 4). Calculations were also carried out by replacing two Ga atoms at sites (No. 1, No. 4) and (No. 1, No. 2) by Mn and, correspondingly replacing the N with C at different sites. Finally, it was found that the ground state configuration is still AFM, in which the two Mn atoms form the nearest neighbor on the surface sites (No. 2, No. 4) with the C at site No.45 binding to the two Mn atoms. But the energy difference between AFM and FM states is considerably reduced (from −0.135 eV/Mn to −0.045 eV/Mn). Thus, we realize that a small concentration of C cannot lead to a transition from AFM to FM states.

We, therefore, increased the hole concentration by replacing more N atoms with C on either sides of the slab. Replacement of two N atoms with C in the $Ga_{36}Mn_4N_{40}$ supercell leads to a $Ga_{36}Mn_4N_{36}C_4$ supercell. We studied six configurations as specified in Table I for the initial Mn sites. For each of these configurations, we replaced two N atoms with C at different sites and calculated the total energies for FM and AFM configurations. It was found that configuration I, in which the two Mn atoms reside at sites (No. 2, No. 4) and C occupy sites (No. 41, No. 45), is the ground state. The FM state lies 0.124 eV lower in energy than the AFM state. The charge density distribution in the plane containing the two Mn atoms, C and neighboring N atoms are plotted in Fig. 3(b). It shows that there is a strong interaction between neighbors Mn and N, and Mn and C atoms which mediate the FM coupling between the two Mn atoms. It is interesting to note that for each of the six initial Mn configurations when two N atoms are replaced by C, the ground state is found to be FM state respectively, and their corresponding energy differences ΔE between AFM and FM range from 0.03 to 0.08 eV/Mn atom. In Fig. 4, we plot the energy difference ΔE and the average magnetic moment on Mn atom for the ground states corresponding to the six initial Mn configurations with the C codoping. For comparison, we also plotted the results for the six configurations before C codoping. Results for the other C-codoped configurations can be provided upon request. Note, there is a significant reduction of the magnetic moment on Mn atoms when the C atoms are codoped. In the ground state, the magnetic moments on the two Mn atoms are $2.15\mu_B$ and $3.04\mu_B$, respectively. Note that the two Mn atoms have different environment. The average magnetic moment of Mn atom is $2.60\mu_B$, as shown in Fig. 4.

The effect of the C concentration on the magnetic coupling between Mn atoms was further examined by replacing three N atoms with C at different sites on the either side of the $Ga_{36}Mn_4N_{40}$ slab. We started with the ground state configuration of $Ga_{36}Mn_4N_{40}$ supercell and then changed the C doping sites to search for the most preferred geometrical and magnetic state. The geometry optimizations and total energy calculations for FM and AFM spin alignment were carried out for all different C codoping configurations. It was found that, in the ground state configuration where the two Mn reside at sites (No. 2, No. 4) and C are at sites (No. 41, No. 42, No. 45), the FM state is lower in energy by 0.237 eV than the AFM state. Once again, we show that the magnetic coupling between Mn atoms changed from AFM to FM when C codoped in the $Ga_{1-x}Mn_xN$ system. More importantly, the FM coupling is enhanced by increasing the C concentration, as the energy difference ΔE is increased (see Table III.

To explore the origin of the FM coupling in C-codoped (Ga,Mn)N, we investigated the electronic structure corresponding to the ground state configuration of $Ga_{36}Mn_4N_{36}C_4$ supercell and compared it with that for $Ga_{36}Mn_4N_{40}$. The calculated total spin DOS, the partial spin DOS for Mn $3d$ and C $2p$, and the partial spin DOS for N atoms in $Ga_{36}Mn_4N_{36}C_4$ are plotted in Figs. $2(c_1)$, $2(c_2)$, and $2(c_3)$, respectively. Comparing the total DOS in Figs. $2(a_1)$, $2(b_1)$, and $2(c_1)$ with each other, we see that there is a significant change of the DOS at the Fermi level. When we dope the Mn atoms in the pure GaN thin film, the energy gap narrows considerably, but the Fermi energy still lies in a region of vanishing electron density. Once we codope C into the (Ga,Mn)N system, we see that the total DOS for spin-up and spin-down are not identical anymore and the energy gap disappears. It clearly shows that the C codoping has introduced new states near the Fermi level resulting in a half-metallic character of this codoped system. This is due to the fact that the Mn atoms in the $Ga_{1-x}Mn_xN$ thin film behave as Mn^{3+} (d^4) state instead of Mn^{2+} (d^5) as found in recent experiment.[28] The Mn^{3+} can readily substitute the group III cation, Ga, without the formation of structural defects or the generation of carriers. In the (Ga,Mn)N codoped with C system, replacing the group V anion, N, with C introduces holes, displaying a strong increase of the Mn spin densities in Fermi level in Fig. $2(c_1)$. These induced hole carriers mediate the interaction of the magnetic ions, Mn, resulting in the FM state. As shown in Fig. $2(b_2)$, without C codoping, neither Mn nor N introduce DOS at the Fermi energy although there is hybridization between the Mn $3d$ and N $2p$ states. However, there is a distinct overlap between Mn $3d$ and C $2p$ in the spin-up bands in Fig. $2(c_2)$ which leads to new states at the Fermi energy and hence results in the change in magnetic coupling. The contribution from N $2p$ to the Fermi sea is negligible, as shown in Fig. $2(c_3)$. Thus, it is clear that the interaction between the localized spins on the Mn ions and delocalized carriers (holes originating from the C valence band) is responsible for the magnetic transition. Preliminary results on Mg codoped (Ga,Mn)N thin film system, shows that there is also a possibility of changing the AFM phase of the (Ga,Mn)N thin film systems to the FM phase. These results will be published elsewhere.

IV. CONCLUSION

In summary, we have carried out a comprehensive study of the electronic structure and magnetic properties of Mn-doped GaN $(10\bar{1}0)$ thin film using spin polarized density functional theory and a slab geometry. We have calculated

the surface relaxation of GaN with and without Mn and have determined the preferred site of Mn and the magnetic coupling between Mn atoms. We find the surface relaxation to be significant, but it does not affect the preferred site of Mn nor the magnetic coupling between them. The Mn atoms prefer to occupy surface sites and cluster around a N atom and couple antiferromagnetically. This property is insensitive to the thickness of the film and the Mn concentration. Our theoretical results are in agreement with the recent experimental observations where the AFM coupling and clustering of Mn in $Ga_{1-x}Mn_xN$ thin films have been reported.[14–19]

Our results on the (Ga,Mn)N system codoped with C suggest that it is possible for the Mn atoms to couple ferromagnetically when the concentration of C is increased to a certain amount. This FM coupling is brought about the hole carriers introduced by C. The density of states in C-codoped (Ga,Mn)N shows half metallic behavior where C introduces states at the Fermi level in the spin-up band. The overlap between Mn 3*d* and C 2*p* leads to the change in the magnetic coupling. Based on this theoretical predication of FM behavior introduced by C codoping, it is not unreasonable to expect that high Curie temperature in FM (Ga,Mn)N thin film can be obtained by optimizing Mn and hole dopant concentration.

ACKNOWLEDGMENT

The work was supported in part by grants from the Department of Energy (DOE). The authors thank the crew of the Center for Computational Materials Science, the Institute for Materials Research, and Tohoku University (Japan), for their continuous support of the HITACH SR8000 supercomputing facility.

[1] H. Ohno, Science **281**, 951 (1998).
[2] T. Dietl, H. Ohno, F. Matsukura, J. Cibert, and D. Ferrand, Science **287**, 1019 (2000).
[3] M. L. Reed, N. A. El-Masry, H. H. Stadelmaier, M. K. Ritums, M. J. Reed, C. A. Parker, J. C. Roberts, and S. M. Bedair, Appl. Phys. Lett. **79**, 3473 (2001).
[4] G. T. Thaler, M. E. Overberg, B. Gila, R. Frazier, C. R. Abernathy, S. J. Pearton, J. S. Lee, S. Y. Lee, Y. D. Park, Z. G. Khim, J. Kim, and F. Ren, Appl. Phys. Lett. **80**, 3964 (2002).
[5] S. Sonada, S. Shimizu, T. Sasaki, Y. Yamamoto, and H. Hori, J. Cryst. Growth **237**, 1358 (2002).
[6] S. S. Seo, M. W. Kim, Y. S. Lee, T. W. Nohb, Y. D. Park, G. T. Thaler, M. E. Overberg, C. R. Abernathy, and S. J. Pearton, Appl. Phys. Lett. **82**, 4749 (2003).
[7] V. I. Litvinov and V. K. Dugaev, Phys. Rev. Lett. **86**, 5593 (2001).
[8] P. Mahadevan, A. Zunger, and D. D. Sarma, Phys. Rev. Lett. **93**, 177201 (2004).
[9] Y. Shon, Y. H. Kwon, S. U. Yuldashev, Y. S. Park, D. J. Fu, D. Y. Kim, H. S. Kim, and T. W. Kang, J. Appl. Phys. **93**, 1546 (2003).
[10] T. Dietl, H. Ohno, and F. Matsukura, Phys. Rev. B **63**, 195205 (2001).
[11] Q. Wang, Q. Sun, P. Jena, and Y. Kawazoe, Phys. Rev. Lett. **93**, 155501 (2004).
[12] C. Liu, F. Yun, and H. Morkoc, J. Mater. Sci.: Mater. Electron. **16** (9), 555 (2005).
[13] Wen Xu and Yong Guo, J. Appl. Phys. **100** (3), 033901 (2006).
[14] M. Zajac, J. Gosk, M. Kamińska, A. Twardowski, T. Szyszko, and S. Podsiadło, Appl. Phys. Lett. **79**, 2432 (2001).
[15] H. Yang, H. Al-Brithen, A. R. Smitha, J. A. Borchers, R. L. Cappelletti, and M. D. Vaudin, Appl. Phys. Lett. **78**, 3860 (2001).
[16] S. Dhar, O. Brandt, A. Trampert, L. Däweritz, K. J. Friedland, K. H. Ploog, J. Keller, B. Beschoten, and G. Güntherodt, Appl. Phys. Lett. **82**, 2077 (2003).
[17] K. Ando, Appl. Phys. Lett. **82**, 100 (2003).
[18] A. Janottia, Su-Huai Wei, and L. Bellaiche, Appl. Phys. Lett. **82**, 766 (2003).
[19] K. H. Ploog, S. Dhar, and A. Trampert, J. Vac. Sci. Technol. B **21**, 1756 (2003).
[20] W. Kohn and L. J. Sham, Phys. Rev. **140**, A1133 (1965).
[21] J. P. Perdew, K. Burke, and M. Ernzerhof, Phys. Rev. Lett. **77**, 3865 (1996).
[22] Y. Wang and J. P. Perdew, Phys. Rev. B **44**, 13298 (1991).
[23] G. Kresse and D. Joubert, Phys. Rev. B **59**, 1758 (1999).
[24] G. Kresse and J. Furthmüller, Phys. Rev. B **54**, 11169 (1996).
[25] H. J. Monkhorst and J. D. Pack, Phys. Rev. B **13**, 5188 (1976).
[26] H. Schulz, K. H. Thiemann, Solid State Commun. **23**, 815 (1977).
[27] J. E. Northrup and J. Neugebauer, Phys. Rev. B **53**, R10477 (1996).
[28] T. Graf, M. Gjukic, M. S. Brandt, M. Stutzmann, and O. Ambacher, Appl. Phys. Lett. **81**, 5159 (2002).